Imaging challenges and processing solutions in the Brazilian Equatorial Margin: A case study in the Barreirinhas Basin

Karine Pereira[1], Yamen Belhassen[1], Erick Tomaz[1], Sonia Domont[1], and Diego Carotti[1]

Abstract

The Barreirinhas Basin is located in northeast Brazil and is part of the Brazilian Equatorial Margin, a new exploration frontier with complex geology. This basin is characterized by a rugose water bottom, a fast carbonate platform, shallow gas pockets, and a complex channel network. All of these elements represent a significant challenge for velocity model building and imaging of the depositional system. From preprocessing to final imaging, high-end technologies were required to meet the processing objectives. The 3D designature and 3D deghosting were crucial to remove bubble energy and ghosts related to canyon diffractions. The velocity model building exploited offset-dependent dip information in the nonlinear slope tomography — i.e., dip-constrained tomography (DCT) — to deal with small-scale lateral velocity variations. The full-waveform inversion, up to 20 Hz, was able to efficiently capture small velocity anomalies and resolve high-spatial-resolution variations that DCT could not totally solve. Even with a detailed velocity model, some dim zones and amplitude variations were still observable in the depth-migrated image. Gas pockets, responsible for the absorption and phase distortion of the seismic signal (commonly denoted by the quality factor of attenuation, Q), were detected and delineated using volumetric Q tomography. The resultant interval Q model was consistent with the geology, and its use was beneficial in a Q-compensating Kirchhoff prestack depth migration.

Introduction

The Barreirinhas Basin is located in the Equatorial Margin of Brazil (Figure 1), a new exploration frontier with promising potential for hydrocarbon discoveries. In 2013, during the 11th Brazilian licensing round, 26 exploration blocks were available for license in this basin due to significant oil and gas discoveries in West Africa, especially in Ghana and Côte d'Ivoire, which have similar geology to the Brazilian coast. The main exploration target for this survey is located in the Cretaceous/Tertiary turbidite system (around 5 km in depth); however, understanding the entire depositional system, including the shallow carbonates and the shelf, is essential to unlocking the complexity of this new exploration frontier.

The geologic evolution of this basin is related to the lithosphere distension events that culminated in the rupture of the Gondwana paleocontinent and consequent formation of the South Atlantic Ocean (Milani et al., 2000). The basins of the Equatorial Margin have a transcurrent tectonic character, with the formation of large zones of fractures parallel to the coast (Zalán, 1985). The stratigraphic evolution of these basins started during the rift phase with a typical deltaic sedimentation on a marine basin, characterized by sandstones and shale deposits. The postrift sequence presents the usual sedimentation of a platform-slope-basin complex, with turbiditic sandstones associated with deepwater sediments, as well as carbonate platforms (Brandão and Feijó, 1994a, 1994b).

In late 2015, a large-scale (14,500 km^2) 3D seismic acquisition survey was conducted to provide a better understanding of the Barreirinhas Basin. The seismic acquisition layout consisted of a variable-depth streamer with 12 cables, each 8 km long, and a nominal streamer separation of 100 m. The shot depth was 7 m, and the receiver depths ranged from 8 to 50 m.

The area covered by the acquisition presents a complex geologic setting. The water column varies from 200 to 3000 m with the shallow part characterized by a rugose seabed with many canyons, a fast carbonate layer, an intricate channel system, and some gas pockets.

In this paper, we show how an enhanced processing sequence and the application of high-end technologies overcame the imaging challenges due to geology, providing high-quality images of the

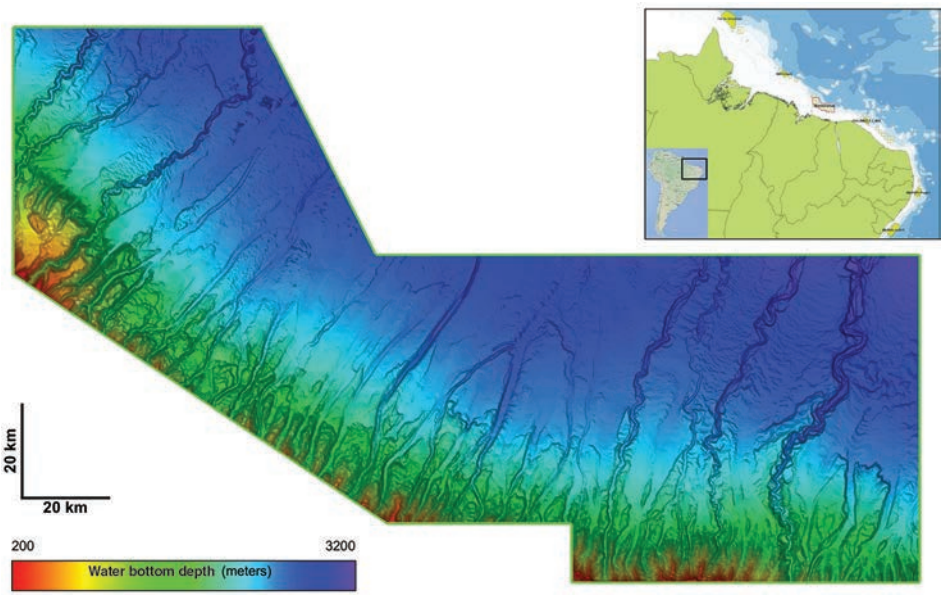

Figure 1. Location of the Barreirinhas Basin and water bottom map of the survey.

[1]CGG.

https://doi.org/10.1190/tle37040283.1.

Barreirinhas Basin. We illustrate the main steps of the processing sequence in a flowchart (Figure 2) that highlights the key processes described in the following sections. We mainly focus on the designature and deghosting flow, the use of dip-constrained tomography (DCT), and full-waveform inversion (FWI) to improve the velocity model building and the final depth imaging using the Q model estimated through Q tomography.

Designature and deghosting

To obtain an accurate representation of the subsurface, source signature and source/receiver ghosts must be removed from the seismic data; 1D designature and 2D deghosting are currently standard practice for processing narrow-azimuth acquisition data. Shallow canyons and carbonate reefs in the Barreirinhas Basin produce significant amounts of out-of-plane energy. The effectiveness of 1D and 2D routines is compromised when dealing with these events, often leading to substantial residual bubble energy and ringing in the seismic response.

1D designature using the vertical far-field signature assumes zero takeoff angle. This can produce reasonable results for near-offset data recorded through the central cables. However, as source directivity is anisotropic, this assumption breaks down and the 1D approximation fails to provide effective removal of bubble energy on far offsets and outer cables.

Receiver deghosting is commonly performed in the linear Radon (τ-p_x) domain, where τ is the intercept time and p_x is the slowness in the inline direction. This approach can separate different emergent angles correctly for in-plane reflections under the 2D assumption. Wang et al. (2013) propose a bootstrap approach that can mitigate some 3D effects, but the method's effectiveness can be degraded for geologic settings where complexities and out-of-plane reflections are considerable.

The main challenges for extending designature and deghosting tools to 3D are the source and receiver spacing in the crossline direction. Aliasing hinders the implementation of 3D linear Radon transforms, which are the basis for accessing takeoff and emergence angle information in seismic data.

Recent advances in 3D deghosting and designature have tried to address this issue, for example Poole et al. (2015) and Wang et al. (2014). These new methods rely on using progressive sparse 3D τ-p_x-p_y transforms, where p_x and p_y are the slowness in inline and crossline directions, respectively. In these transforms, lower frequencies guide higher frequencies to avoid aliasing in the cable direction. This allows for accurate representation of emergence angles and, in turn, effective receiver deghosting. For source designature and deghosting, the sail line spacing is too large for this methodology to work properly. Assuming symmetry between slowness in source and receiver domains, an estimate of the takeoff angle can be made and 3D source deghosting and designature can be applied.

On the Barreirinhas data set, the 2D deghosting flow provided reasonable results in some areas. However, in the shallow part of the basin, where the water bottom is rugose and multiple canyons are present, ghost removal was challenging. Ringing artifacts, especially close to the diffraction tails, were a common observation. 1D designature results were also suboptimal around the shallow

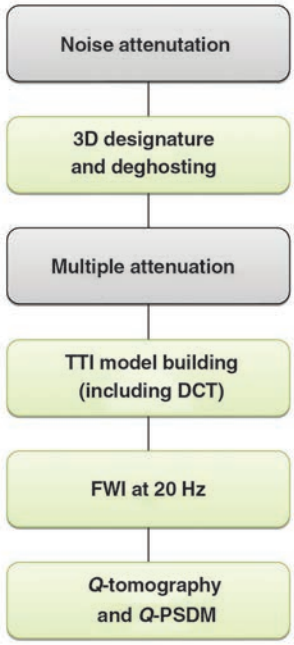

Figure 2. Flowchart of the main steps of the processing sequence. The steps highlighted in green are the key processes described in this paper.

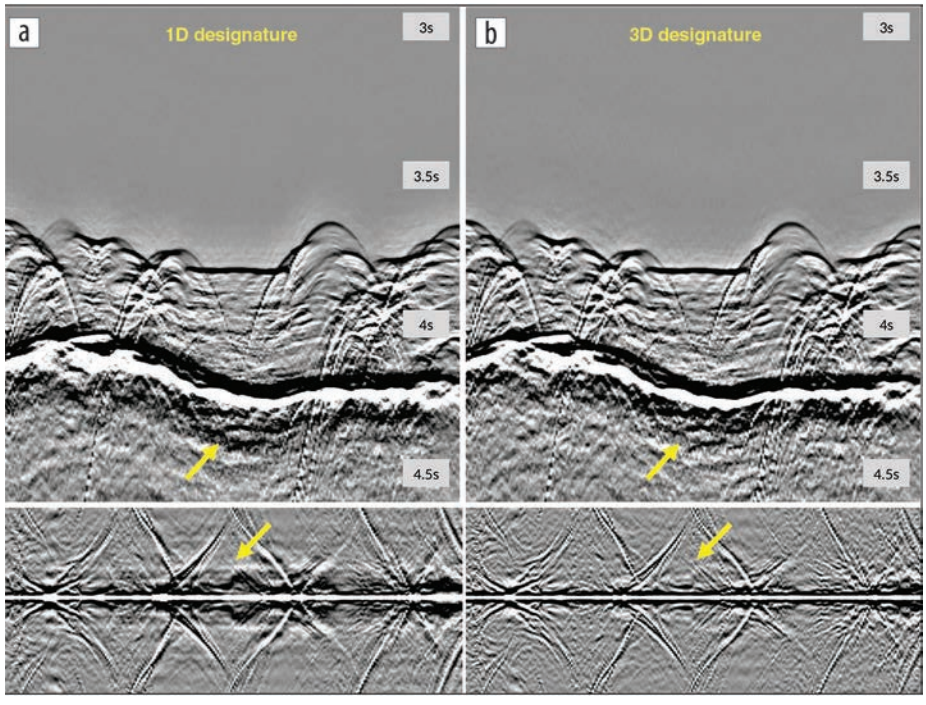

Figure 3. Common channel display comparison between (a) 1D and (b) 3D designature. The lower panels show autocorrelation displays. The yellow arrows show improvements due to 3D designature.

part of the survey because a wider range of takeoff angles is present. Considerable residual bubble energy remained in the data. The solution to this problem was to use the 3D approach, applying joint 3D designature and source deghosting, followed by 3D receiver deghosting. The 3D designature operator was obtained from near-field hydrophone data (Ziolkowski et al., 1982).

Figure 3 shows a common channel section characterized by a rugose water bottom. Multiple diffraction tails can be seen. The comparison demonstrates that the 3D source designature approach better removed the bubble energy when compared to the 1D filter, with the autocorrelations confirming this observation. As mentioned earlier, 2D deghosting can introduce ringing around the diffraction tails. In Figure 4, 2D deghosting artifacts are still visible after migration, compromising the quality of the final image, while the 3D results appear more stable. Overall, a more reliable and stable result was achieved with 3D designature and 3D deghosting.

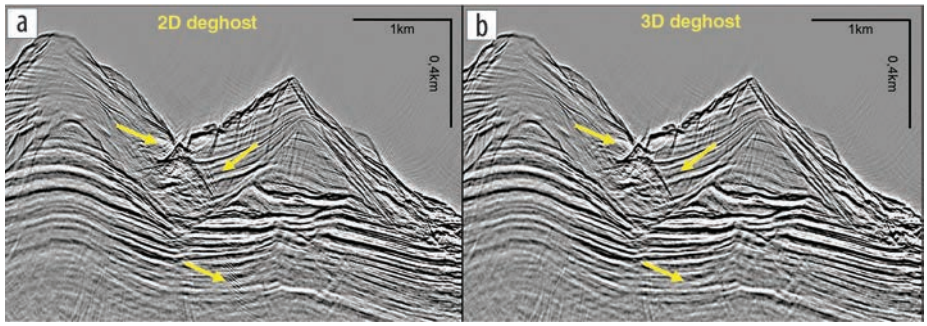

Figure 4. Migrated data with (a) 2D deghosting and (b) 3D deghosting. Ringing artifacts are visible after migration in the 2D flow, as indicated by the yellow arrows, which are mitigated in the 3D approach.

Dip-constrained tomography

Velocity model building in this area is a challenge and, for large unexplored plays with limited or no well information, a smooth tomographic inversion is often the first choice. This process relies on the quality of curvature picking on migrated gathers, commonly known as residual moveout (RMO).

For the Barreirinhas Basin, a shallow high-velocity carbonate layer is present. The variable thickness of this layer correlates with the shape of the seabed canyons. This lateral variation introduces strong velocity contrasts as the geology alternates between the fast carbonates and the slower sandstones surrounding them. Depending on the wavelength of these carbonate bodies, lateral velocity variations might not be sufficiently captured with conventional tomography. The resultant model can cause distortions (pull up/push down) in deeper layers below the canyons and hence have a direct impact on interpretation. Higher density RMO picking with high-resolution tomography could be proposed as a solution, but the results would still be compromised because the fast carbonate layer hinders our ability to pick reliable RMO information due to excessive stretch at mid and far offsets.

To address these challenges, an approach that utilizes dip information as well as RMO information was adopted. Guillaume et al. (2013) propose DCT to resolve high wavenumber features such as channels. The aim of DCT is to find the velocity model that best minimizes both the RMO and the misfit between the structural dip of different offsets. Dips across different partial stacks, as well as selected reliable RMO picks, were picked on the Barreirinhas data set. Both types of picks were then used within a multilayered (Guillaume et al., 2012) DCT scheme. The high-velocity carbonate layer is defined separately to avoid contaminating updates elsewhere in the model.

Figure 5 compares tomographic inversion results with conventional tomography and DCT. Without DCT, an undulation in the deeper part was observed due to the inaccuracy of the velocity model (Figures 5a and 5c). DCT improves the velocity model in the carbonate layer with a significant impact on the deeper image (Figures 5b and 5d). Using DCT, it was possible to obtain a better velocity model for the carbonate layer, capturing most of the lateral variation and high velocity of these rocks. DCT also helped delineate some low-velocity anomalies in the shallow part related to free gas zones. The red ovals in Figure 5 highlight the image improvements. The gathers shown in Figure 6 demonstrate that DCT provided both flatter events and more plausible structural images. Although the main improvements in the velocity model were in the shallow part, the flatness of gathers and the focusing of events were improved in the deeper section as well.

Full-waveform inversion

As mentioned earlier, the Barreirinhas geology is characterized by shallow gas pockets above a complex carbonate platform. DCT helped obtain a reasonable velocity update within the carbonate platform. Higher resolution was needed to find the correct velocity of the shallow gas pockets and to correctly image the events inside the carbonates. With the obtained DCT model, because there was limited reliable RMO information in some locations within these layers, it was decided to run FWI in the most complex area of the project. FWI is an iterative technique whereby the velocity of the subsurface is updated by comparing the acquired seismic data with synthetic data (Tarantola, 1984). These synthetic data are created by forward propagating a wavelet (that represents the source signature) through an initial velocity model. The objective function used here measures the residual difference between synthetic and observed data. It requires the starting velocity model to be reasonably close to the true model and utilizes low frequencies such that the modeled and real field data are not cycle skipped — namely, they do not differ by more than half a cycle in their arrival times. Any differences are assumed to be velocity errors and are used to update the initial velocity model.

In the Barreirinhas project, the acquisition is narrow azimuth and has a maximum offset of 8.2 km. Due to the high reflectivity of the carbonate layer, diving waves had limited penetration, but the rich refractions helped delineate the gas bodies and the top of carbonate. The main challenge in Barreirinhas FWI is cycle skipping. To overcome this, first forward modeling was performed to evaluate the starting model, then the synthetic shots were compared to their real counterparts to evaluate the cycle-skipping issue. In some areas, there was a mismatch of more than a full cycle.

Uncertainties at this point had multiple origins: phase distortion through gas pockets, anisotropy inaccuracy, and velocity errors. Next, the anisotropy was updated using tomography to provide a better starting point for FWI. With this change, it was possible to see a better match at further offsets, suggesting that the mismatch was not just velocity inaccuracy. Overall, the edited final anisotropic velocity model gave an acceptable initial synthetic-to-real data match. Next, FWI with an offset striping approach was used to further mitigate cycle skip. FWI was performed gradually from 4 to 20 Hz, which improved resolution in the final model.

Kirchhoff prestack depth migration (PSDM) test lines showed improved gather flatness and imaging, especially around the base of carbonate. Figure 7 compares the tomographic final result with the FWI final model. Using FWI, a better velocity model is obtained for the carbonate layer, located between the red dashed curve (top of carbonate) and the blue dashed curve (base of carbonate). Most of the lateral variation and the high velocity of these rocks were captured, even correcting the contrast position, suggesting a different top of carbonate compared to the initial interpretation (black oval). FWI also delineates many low-velocity anomalies in the shallow part related to free gas zones (yellow arrows). The deeper part shows more continuous geology, suggesting a reasonable inversion result for the upper part of the model (white oval showing better positioning of the base of carbonate). Figure 8 shows the comparison between the gathers migrated with the final tomography velocity and with the FWI velocity, the latter being flatter overall.

Depth velocity slices show various anomalous features that correlate well with the geology. Figure 9 shows the comparison of a depth image slice overlaid with the final tomography and the

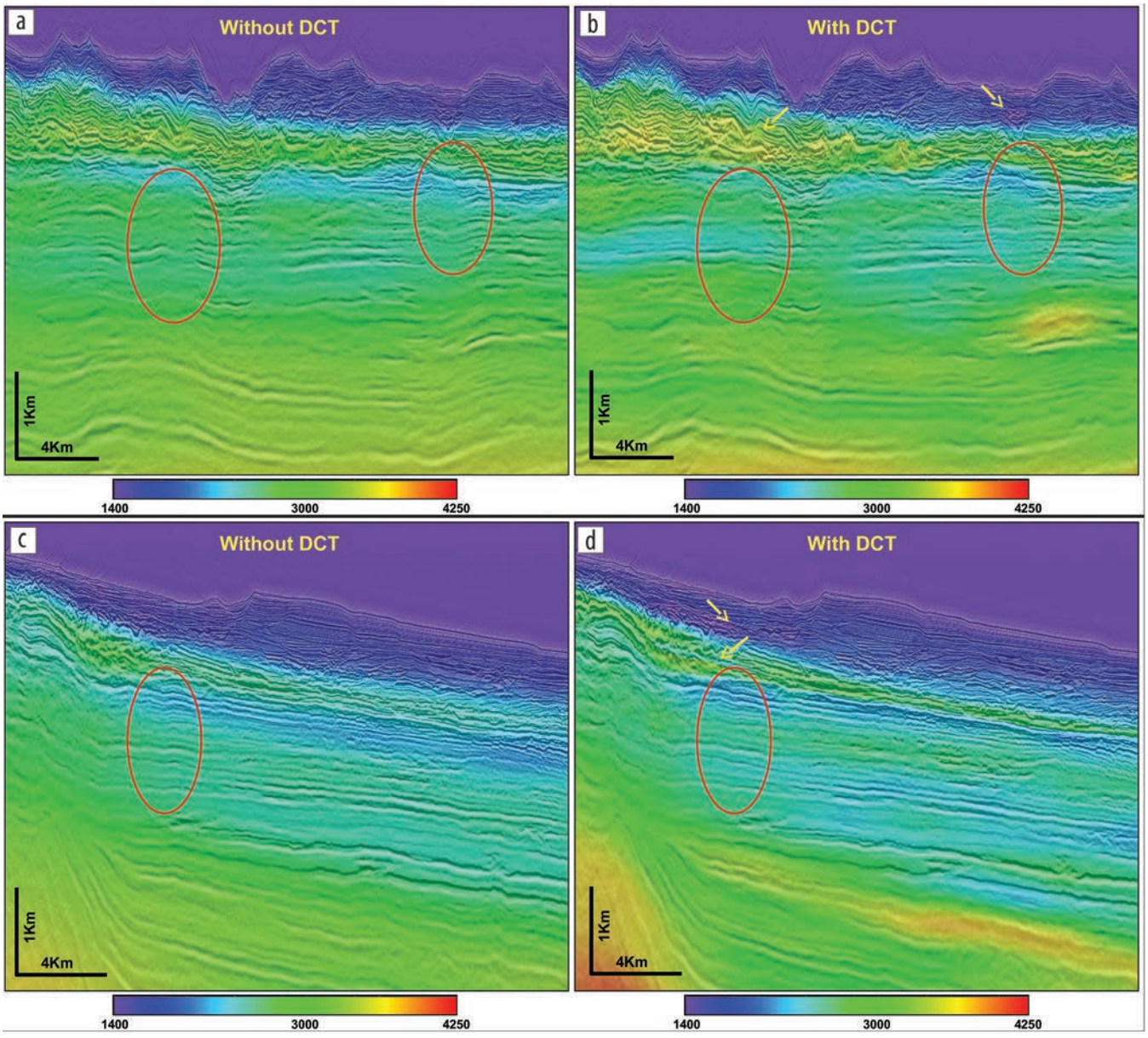

Figure 5. Stack image overlaid with velocity model without and with DCT, respectively, for (a) and (b) inline view and (c) and (d) crossline view. The red ovals indicate the improvements on the seismic image with DCT and the yellow arrows indicate the velocity changes that helped to improve the image.

final FWI model. The gas pocket with low velocity is indicated by the yellow arrow.

Q tomography and *Q* PSDM

Preprocessing through 3D designature and deghosting, and the better velocity model acquired by DCT and FWI, helped produce a better image of the subsurface. However, lateral amplitude variations and amplitude dim zones were still present after Kirchhoff PSDM. The very low velocities (even lower than water velocity), captured by FWI just above these areas with weak amplitude and the presence of the bottom simulating reflection (BSR), are a clear indication of strong absorption due to free gas. The BSR is the physical (not lithological) interface between gas hydrate and free gas. It has the shape of the water bottom with a reverse polarity and crosscuts the strata reflections. Figure 10 shows a depth slice where the BSR is easily identified, as indicated by yellow arrows.

Amplitude loss is the most visible effect of absorption (Q) in seismic data, but it is not the only one. The other effect is phase distortion, which is responsible for incorrect positioning of seismic events and the subsequent loss of resolution due to reduced focusing. It is important to compensate the absorption effects to provide a high-resolution seismic image with good interpretability. In exploration areas with limited well information, like the Barreirinhas Basin, Q compensation is usually performed using a constant Q model that is able to balance the amplitude between the shallow and deep parts. But in this survey, the free gas causing strong absorption is localized in some small areas. Hence, the seismic image suffers from nonhomogeneous amplitude attenuation and phase distortion that a constant Q model cannot handle, so a 3D geologically consistent Q model is necessary for capturing the absorption variation.

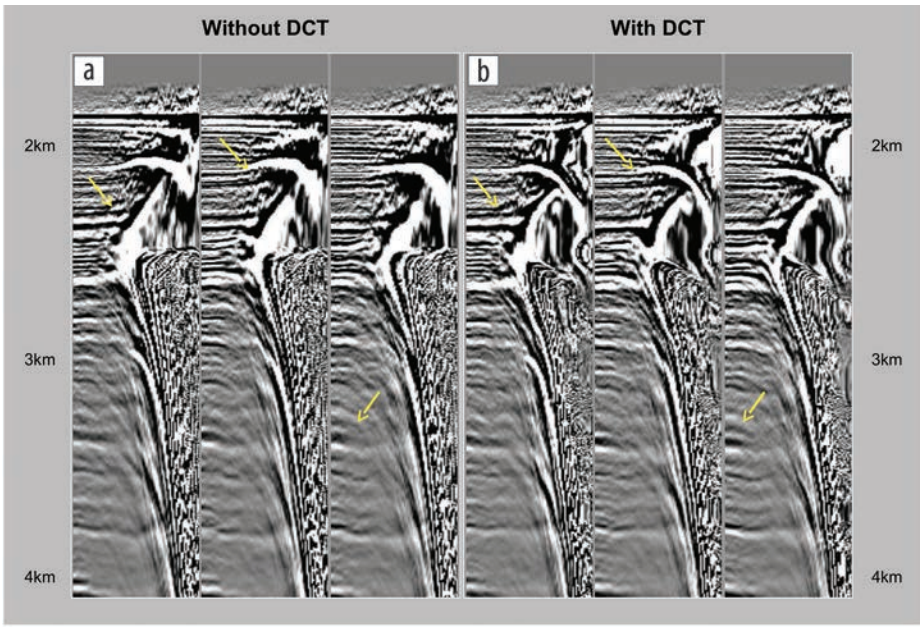

Figure 6. Common image gathers (a) without and (b) with DCT. The yellow arrows indicate improvements on the gather flatness due to DCT.

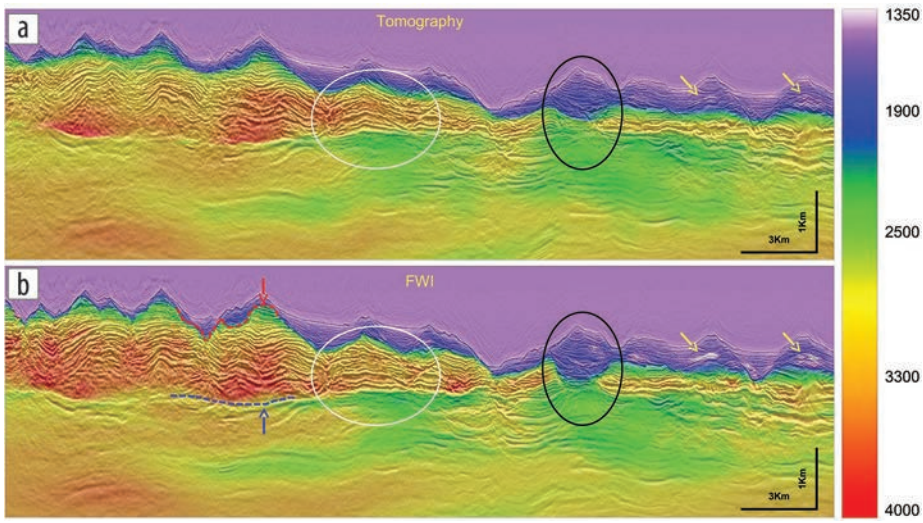

Figure 7. Stack image with corresponding velocity model overlaid: (a) tomography and (b) FWI. The red dashed curve and the red arrow indicate the top of carbonate. The blue dashed curve and the blue arrow show the base of carbonate. The yellow arrows point to gas pockets better localized by FWI. The white oval shows improvements in the position of the base of carbonate after FWI. Finally, the black oval indicates an area where FWI velocity contrast suggests a different position of the top of carbonate.

Estimation of the Q model for this survey was done using the frequency peak shift (FPS) method and volumetric Q tomography (Gamar-Sadat et al., 2015). The proposed flow is able to estimate a background Q model while localizing small anomalies, especially ones related to gas. Because higher frequencies are absorbed faster than lower frequencies, the frequency peak of the spectrum (namely the frequency with the highest amplitude) is shifted toward the lower frequencies as traveltime increases. Starting from this observation, the FPS method aims to estimate the effective Q based on the frequency peak of the amplitude spectrum in different time windows. Computing the effective Q for different offset classes, a four-dimensional effective Q volume (time, inline, crossline, and offset) was obtained. Finally, a volumetric Q tomography inverted these measurements to obtain a 3D interval Q model.

The Q model obtained with Q tomography was conformal to the geology and captured the Q anomalies related to gas pockets without any a priori information on their locations; strong Q anomalies were automatically detected and positioned above the dimming zones.

To assess the validity of the *Q* model in this exploration area, an amplitude variation with offset (AVO) analysis was performed. Following AVO theory, sandstones saturated with gas are expected to have an AVO class 3 response, characterized by a positive product of AVO intercept and gradient. This attribute is shown in Figure 10a and has positive (red) values along the BSR and correlates well with the *Q* anomalies related to gas (Figure 10b). Small *Q* values, namely regions of strong absorption, can be observed inside the area bordered by the BSR and are highlighted by red ovals.

Once a reliable interval *Q* model had been obtained from *Q* tomography, *Q* compensation was applied by considering the raypath during migration; *Q*-Kirchhoff PSDM was used for this case study. The difference between conventional Kirchhoff PSDM and one using *Q* relates to the traveltimes used in the algorithm. While the conventional method uses conventional traveltimes, *Q* migration uses complex traveltimes that carry the information to compensate both the amplitude attenuation and the phase distortion. Figure 11 shows the comparison between conventional Kirchhoff PSDM and *Q*-Kirchhoff PSDM for one inline and one crossline. The interval *Q* model follows the geology and captures very nicely the *Q* anomalies in the shallow part. The deeper regions below the gas pockets are better imaged with higher resolution because the *Q* migration is compensating for the absorption along the full raypath. The lateral amplitude behavior is better balanced on the *Q* PSDM when compared to the conventional result. The areas below the *Q* anomalies have amplitudes closer to the surrounding areas less affected by strong absorption and the base of carbonate is more continuous. The yellow arrows show some of the improvements in the *Q* PSDM image.

Compensation inside the migration algorithm allows better common image gathers, which facilitates all the successive prestack processes. Some events barely seen in the conventional migration are properly imaged with *Q* PSDM. The extent of the improvements with *Q* PSDM using the volumetric *Q* model obtained with *Q* tomography is also noticeable on the depth slice shown in Figure 12. The seismic events become more continuous, and many structures are better focused.

Conclusions

The Barreirinhas Basin is a promising play that requires high-quality images of the subsurface to allow the best interpretation of the area. The use of high-end technologies in the processing sequence improves the quality of the seismic data to provide higher resolution, better amplitude balancing, and good positioning of the seismic events. These technologies are

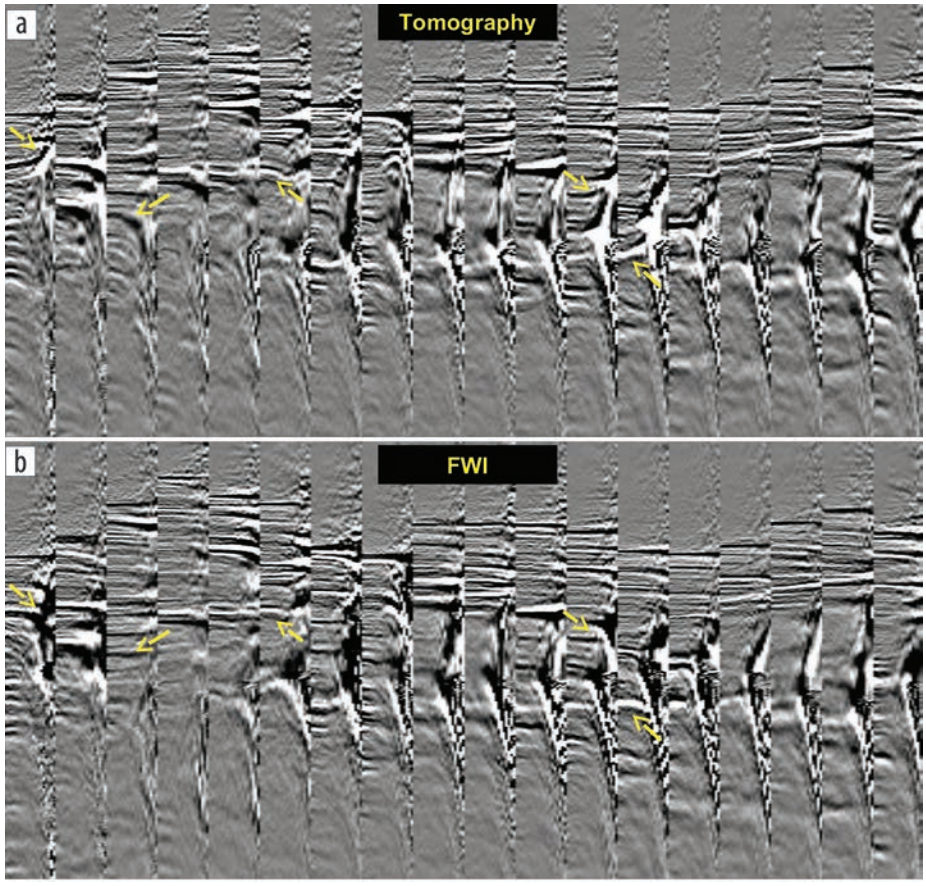

Figure 8. Gathers migrated with velocity model from (a) tomography and (b) FWI. The yellow arrows indicate the better flatness of gathers with the FWI velocity model.

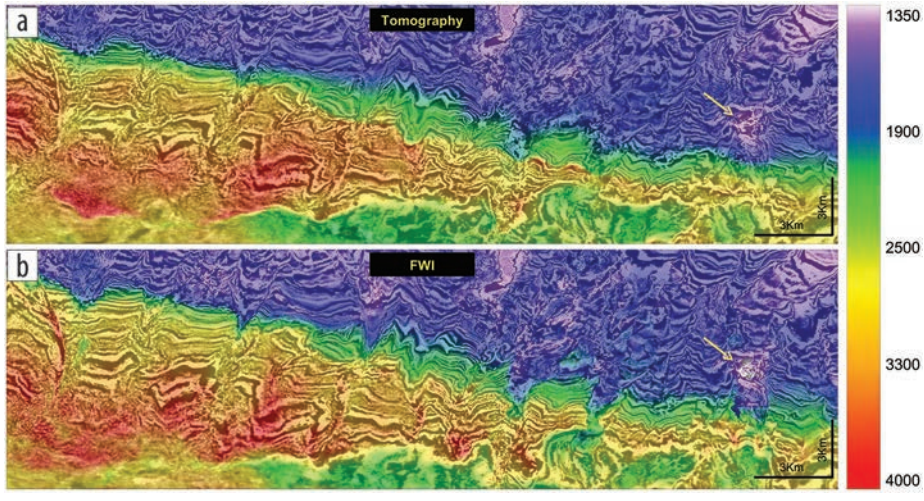

Figure 9. Depth slices of stack image and corresponding velocity model (a) tomography and (b) FWI. The yellow arrow shows the gas pocket.

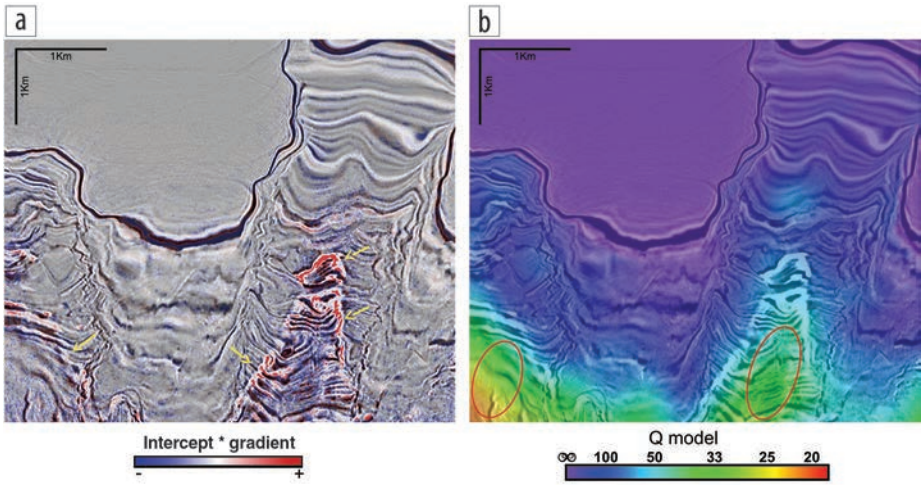

Figure 10. Stack image depth slice around the BSR overlaid with (a) AVO product and (b) *Q* model. The yellow arrows indicate the BSR, and the red ovals show the areas with small *Q* values (strong attenuation) bordered by the BSR.

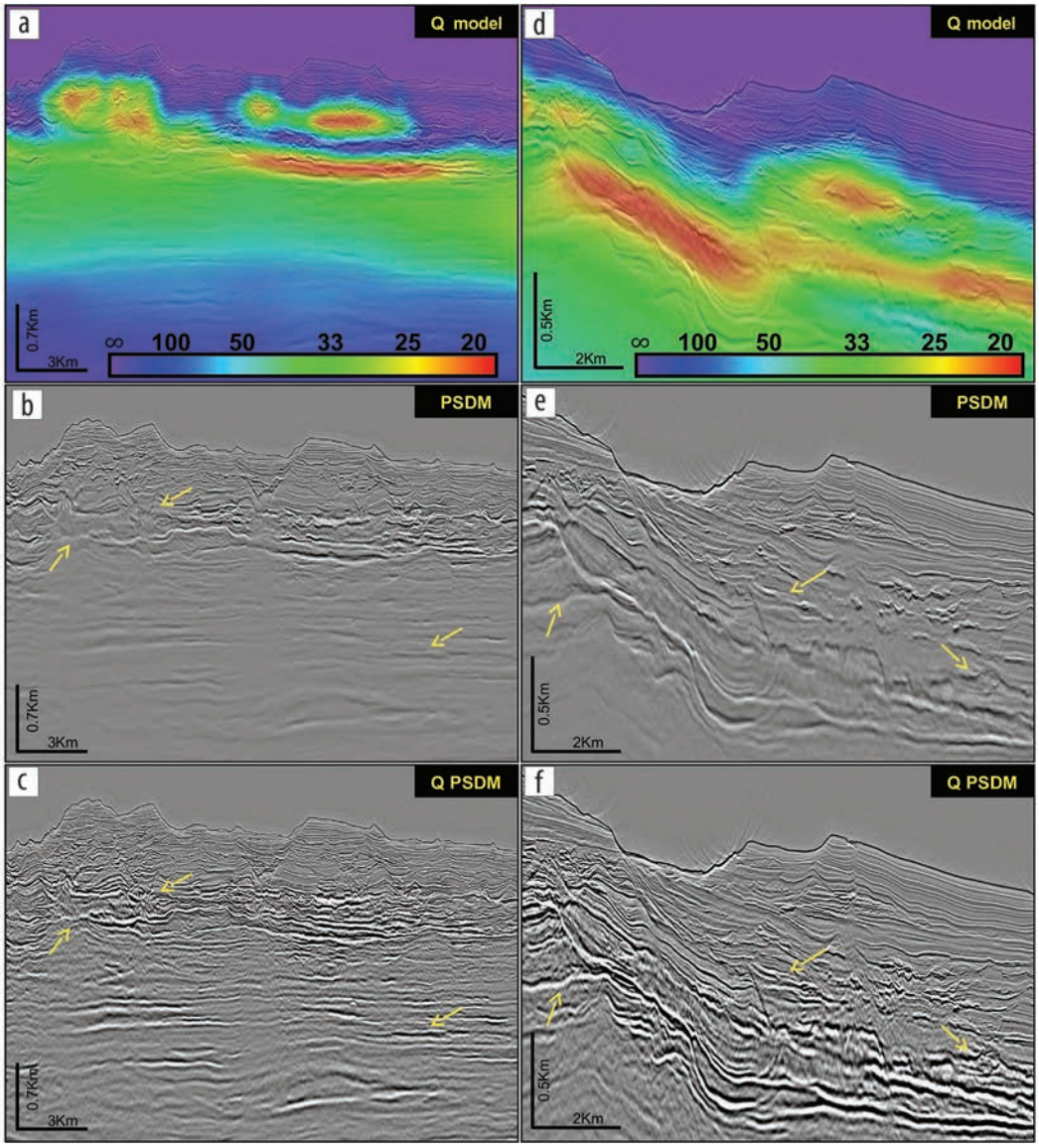

Figure 11. *Q* model and stack image comparison of conventional Kirchhoff PSDM and *Q*-Kirchhoff PSDM: (a–c) inline view and (d–f) crossline view. The yellow arrows indicate some of the improvements with *Q* PSDM compared to conventional PSDM.

necessary to overcome the geologic complexity of this basin: (1) 3D designature and 3D deghosting to exploit the full bandwidth of the seismic data with no visible notches; (2) DCT and FWI to obtain a reliable velocity model of the canyons, channels, and shallow carbonate layer; and (3) imaging with *Q* PSDM to compensate for strong absorption caused by free gas, using a geologically consistent *Q* model from *Q* tomography. This broadband processing contributed to better amplitude recovery, better lateral amplitude balancing, and increased resolution in the final imaged data. Finally, we highlight that the obtained *Q* model could also be important to identify shallow hazard areas, especially gas, that are best avoided while drilling a well.

The strong absorption caused by *Q* anomalies can cause considerable phase distortion. In the time domain it is seen as a time shift, which could be an issue for FWI because the mismatch between synthetic and real data could be due to phase distortion and not velocity inaccuracy. To avoid this, it would be interesting for future work to perform iterative *Q* tomography and FWI or even a joint inversion of *Q* and velocity with *Q* FWI. This approach could provide even more accurate *Q* and velocity models. TLE

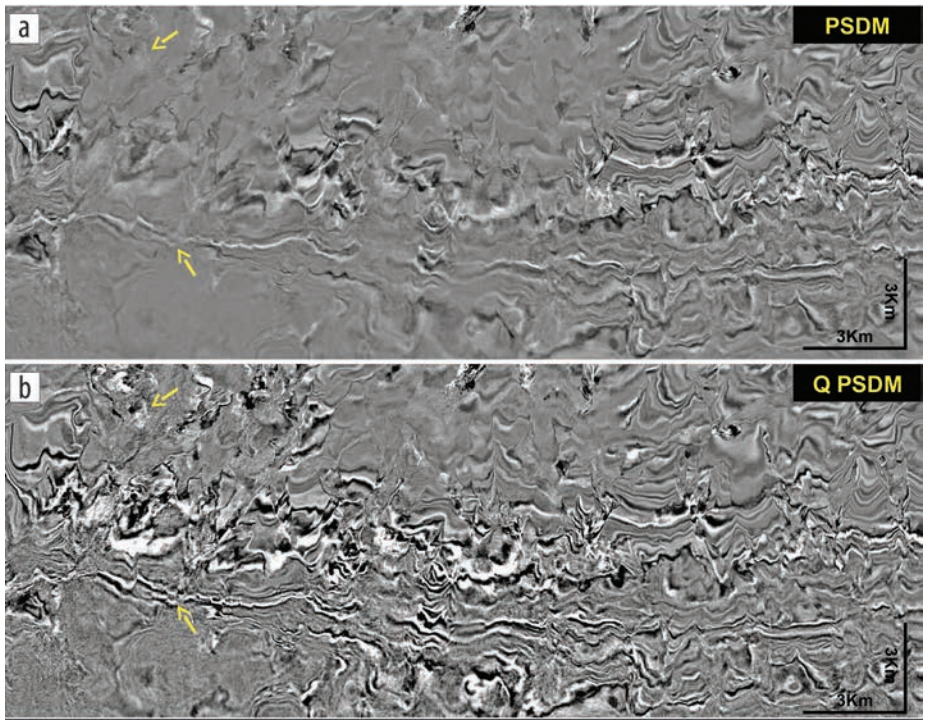

Figure 12. Stack image depth slice comparing (a) conventional Kirchhoff PSDM and (b) *Q*-Kirchhoff PSDM. The yellow arrows indicate some of the improvements with *Q* PSDM compared to conventional PSDM.

Acknowledgments

We would like to thank CGG Multi-Client & New Ventures for their permission to publish this work and Fatiha Gamar for her support in the *Q* tomography tests.

Corresponding author: diego.carotti@cgg.com

References

Brandão, J. A. S. L., and F. J. Feijó, 1994a, Bacia da Foz do Amazonas: Boletim de Geociências da Petrobras, **8**, no. 1, 91–99.

Brandão, J. A. S. L., and F. J. Feijó, 1994b, Bacia do Pará-Maranhão: Boletim de Geociências da Petrobras, **8**, no. 1, 101–102.

Gamar-Sadat, F., P. Guillaume, A. Pica, G. Pignot, P. Poggi, A. Henry-Baudot, A. Prescott, A. Gacha, D. Carotti, and V. Prieux, 2015, Automatic gas pockets detection by high-resolution volumetric Q-tomography using accurate frequency peak estimation: 77th Conference and Exhibition, EAGE, Extended Abstracts, https://doi.org/10.3997/2214-4609.201413251.

Guillaume, P., S. Hollingworth, X. Zhang, A. Prescott, R. Jupp, G. Lambaré, and O. Pape, 2012, Multi-layer tomography and its application for improved depth imaging: 82nd Annual International Meeting, SEG, Expanded Abstracts, 1–5, https://doi.org/10.1190/segam2012-0683.1.

Guillaume, P., M. Reinier, G. Lambaré, A. Cavalié, M. I. Adamsen, and B. M. Bruu, 2013, Dip-constrained non-linear slope tomography: An application to shallow channel characterization: 75th Conference and Exhibition, EAGE, Extended Abstracts, https://doi.org/10.3997/2214-4609.20130368.

Milani, E. J., J. A. S. L. Brandão, P. V. Zalán, and L. A. P. Gamboa, 2000, Petróleo na margem equatorial Brasileira: Geologia, exploração, resultados e perspectivas: Brazilian Journal of Geophysics, **18**, no. 3, 351–396.

Poole, G., J. Cooper, S. King, and P. Wang, 2015, 3D source designature using source-receiver symmetry in the shot tau-p_x-py domain: 77th Conference and Exhibition, EAGE, Extended Abstracts, Th-N103-13, https://doi.org/10.3997/2214-4609.201413193.

Tarantola, A., 1984, Inversion of seismic reflection data in the acoustic approximation: Geophysics, **49**, no. 8, 1259–1266, https://doi.org/10.1190/1.1441754.

Wang, P., S. Ray, C. Peng, Y. Li, and G. Poole, 2013, Premigration deghosting for marine streamer data using a bootstrap approach in tau-p domain: 83rd Annual International Meeting, SEG, Expanded Abstracts, 4221–4225, https://doi.org/10.1190/segam2013-0225.1.

Wang, P., S. Ray, and K. Nimsaila, 2014, 3D joint deghosting and crossline interpolation for marine single-component streamer data: 84th Annual International Meeting, SEG, Expanded Abstracts, 3594–3598, https://doi.org/10.1190/segam2014-0882.1.

Zalán, P. V., 1985, Tectonics and sedimentation of the Piauí-Camocin sub-basin, Ceará Basin, offshore northeastern Brazil: Petrobras, Serie Ciência-Técnica-Petróleo 17.

Ziolkowski, A., G. E. Parkes, L. Hatton, and T. Haughland, 1982, The signature of an air-gun array: Computation from near-field measurements including interactions: Geophysics, **47**, no. 10, 1413–1421, https//doi.org/10.1190/1.1441289.